Published in the Proceedings of the 16th International Aluminum Alloys Conference (ICAA16) 2018
ISBN: 978-1-926872-41-4
by the Canadian Institute of Mining, Metallurgy & Petroleum

EVALUATION OF THE LATERAL CRUSH PERFORMANCE OF Al-Mg-Si EXTRUSIONS

*J-F. Béland[1] and N. Parson[2]

[1]*National Research Council Canada (NRC)*
501 Université Est blvd
Saguenay, Québec, Canada, G7H 8C3
*(*Corresponding author: Jean-Francois.Beland@cnrc-nrc.gc.ca)*

[2]*Rio Tinto Aluminium*
Arvida Research and Development Centre
Saguenay, Québec, Canada, G7S 4K8

ABSTRACT

The design of extruded aluminum crash structures including crash rails, crash cans, bumpers and structural body components is dependent on the mechanical behavior of the materials used in these components along with other specific requirements such as the stored energy level, maximum allowable crush force and space available for the structure. The main design objective of crash structures is to maximize the energy absorption capability while also minimizing part weight. Alloy and temper selection play a vital role in increasing the energy absorbed-to-weight ratio of a part since the profile shape and thickness are determined by the material's extrudability, strength and ductility. The axial crush behavior of Al-Mg-Si extrusions has been widely studied, including work by the current authors, and a visual ranking system is typically used in the industry. However, information pertaining to material performance in the case of *lateral* crush, relevant to intrusion beams or side sills, is still limited. This paper focuses on the development of a lateral crush test protocol and presents an evaluation of the transverse crush performance of common Al-Mg-Si alloys.

KEYWORDS

Aluminum, 6XXX series, Crash, Crush, Extrusions, Impact, Toughness

INTRODUCTION

In recent years, aluminum extrusions have gained increased used in crash management systems, thanks to their superior specific energy absorption capabilities, as compared to steel. Moreover, Al-Mg-Si alloys (6XXX series) can be readily extruded into the complex hollow profiles needed for these crash management systems; this is especially true for the front-impact management system where aluminum extrusions are well-suited to meet the desired crash behavior of the bumper and crash boxes.

While the axial crush behavior of Al-Mg-Si extrusions has been widely investigated, including work carried out by the present authors [1-5], literature regarding the material performance in the case of lateral crush for intrusion beams or side sills is still limited, in spite of the fact that side impact is more critical with respect to occupant safety due to the smaller space available for the crush zone and, as a result, there is less room for energy absorption prior to cabin intrusion. To date, a handful of crash studies have been carried out on the design of side crash components, particularly the anti-intrusion beam located in the front doors [6-9], providing various solutions and testing methods for side impact performance. As the design of intrusion beams and side sills is different from one vehicle to another depending on the material and manufacturing techniques, evaluation methods of material properties may differ according to the adopted design strategy. The current study focuses on the use of hollow aluminum extrusions.

The two most critical scenarios for lateral crash are (i) a side impact from another vehicle and (ii) a side impact into a pole or a tree. In both cases, the role of the intrusion beams and side sill is to stiffen the structure and transfer the impact loads to the other structural members of the chassis, while being able to absorb energy over a short distance. The design of these structural members using aluminum extrusions requires a full understanding of the influence of alloy chemistry and extrusion parameters on material strength and ductility in order to stiffen the structure as needed, while lowering vehicle weight and maintaining good energy absorption. On the other hand, the use of medium to high strength Al-Mg-Si alloys with improper extrusion parameters can lead to inadequate load bearing during a side impact, due to insufficient ductility of the material.

The present paper summarizes the development of a lateral crush test protocol, coupled with material strength and ductility evaluations obtained from various mechanical tests, to investigate the lateral crush performance of a number of common press quenched 6XXX aluminum alloys in a variety of tempers.

EXPERIMENTAL PROCEDURE

Four alloy compositions were DC cast as 101 mm diameter billets, homogenised according to standard commercial practices and extruded on the RTA 780-tonne experimental press. The alloys chosen for this study were (i) 6063GP, which is a general purpose AA6063 alloy typically used to meet AA6063 T6 requirements, (ii) 6063HS, which is a high strength variant of AA6063 developed to meet the AA6063 T65 minimum properties, and (iii, iv) standard AA6061 and AA6082 representing higher strength 6XXX alloys. The latter utilise sub-micron dispersoid forming additions to control the microstructure and the associated mechanical properties. These four materials were press-quenched using a water-spray quenching unit located ~1.5 m from the die. This quenching unit was jointly designed by the NRC and Rio Tinto in order to simulate spray cooling rates typically encountered in industry. Figure 1 shows the quenching unit in operation in Rio Tinto′s extrusion laboratory. This unit is equipped with four cooling lines where the water flow rate can be modified for each line independently. Various types of nozzles can also be used to modify the cooling rate and water-spay pattern. For this particular study only the top and bottom cooling lines were used. The type of nozzle used produced a full cone with 60° angle. The distance between two adjacent nozzles and the distance between the extrusion profile and the nozzle line was set such that the "front half" of a given spray cone overlapped with the "back half" of the preceding cone. The quench rate was measured using a clip on wireless data logger, as ~20°C/s in the critical range of 500°C-250°C, as shown in Figure 2. Heat treatments covering underaged to overaged tempers were developed for temperatures of 175 to 200°C, and times up to 8 hrs, to produce various levels of strength and ductility. Details of these heat treatments are provided in Table 1.

Figure 1. Quenching unit in operation in the Rio Tinto extrusion laboratory.

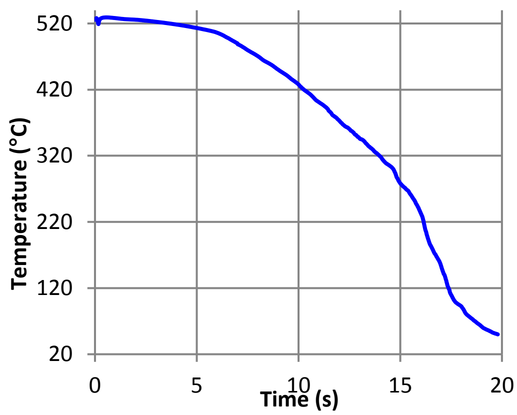

Figure 2. Quench curve obtained from the extrusion quenching unit.

The alloy/temper combinations described earlier were then tested using a lateral crush test protocol developed to quantify the energy absorption and qualitatively assess the ductility, with respect to crash applications. Quasi-static testing was selected as the strain rate sensitivity of aluminum alloys at ambient temperature is low, although it is possible to apply a small dynamic factor to better approximate the gain in crash force due to impact velocity.

Table 1. Heat treatments performed on the extruded 6XXX alloy profiles (U = underaged, P = peak-aged, O = overaged).

T (°C)	175			200	
Time (h)	3	5	8	2	3
6063		U	P	O	
6063HS		U	P	O	
6061	U		P		O
6082	U		P		O

Profile Geometry and Lateral Crush Test Protocol Selection

The shape and dimensions of an extruded section have a great influence on the deformation behaviour and amount of strain generated in a lateral crush test. For side sills, the objective is to stiffen the beam with internal webs and to rely on the proper folding of the walls to withstand high loads and absorb energy. The lateral crush test used in this work consisted of a 50 mm punch with a 25 mm end radius crushing an extruded profile, as shown in Figure 3. As can be seen from the image, the bottom of the extruded profile was fixed to a plate while the top surface was fixed at each end of the tube in order to increase the level of strain experienced by the upper surface. As no bending is allowed, this setup better represents the lateral crash behavior of a side sill, but with significant localized deformation. In the case of an intrusion beam, bending would be applied to evaluate the tensile resistance of the bottom surface.

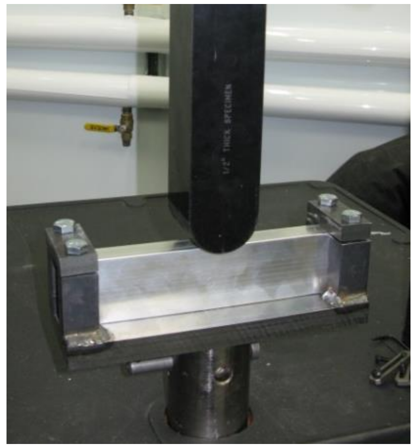

Figure 3. Lateral crush setup.

The extruded section chosen for the present work was a single-cell rectangular profile. The lateral crush behavior of this section was examined using a FE model in order to determine the wall thickness and overall dimensions to obtain the desired extrusion ratio and crush stability. Previously, the current authors were able to model the damage and fracture of a 6008-T6 alloy with a fast quench rate (~1000°C/s), giving a more ductile material than with the usual quench rates found in the industry. The material model was elastic-plastic with isotropic properties and was coupled to damage evolution criteria in order to predict the onset of fracture as a function of the loading path. The commercially available Ls-Dyna package was used for the simulations. This model was used to evaluate various widths, heights, corner radii and wall thicknesses. Figure 4 presents the simulation results for lateral crush behavior with 5 mm and 1 mm corner radii and Figure 5 shows the resulting force versus crush displacement response. Too large a corner radius for a given width and height will significantly change the instability and deformation of the walls leading to premature fracture and low energy absorption. For this case, an increase of 65% in energy absorption can be achieved by having the proper crush behavior with the small (i.e. 1 mm) corner radius. This radius is close the limit to avoid corner tearing during commercial extrusion of medium strength 6XXX alloys.

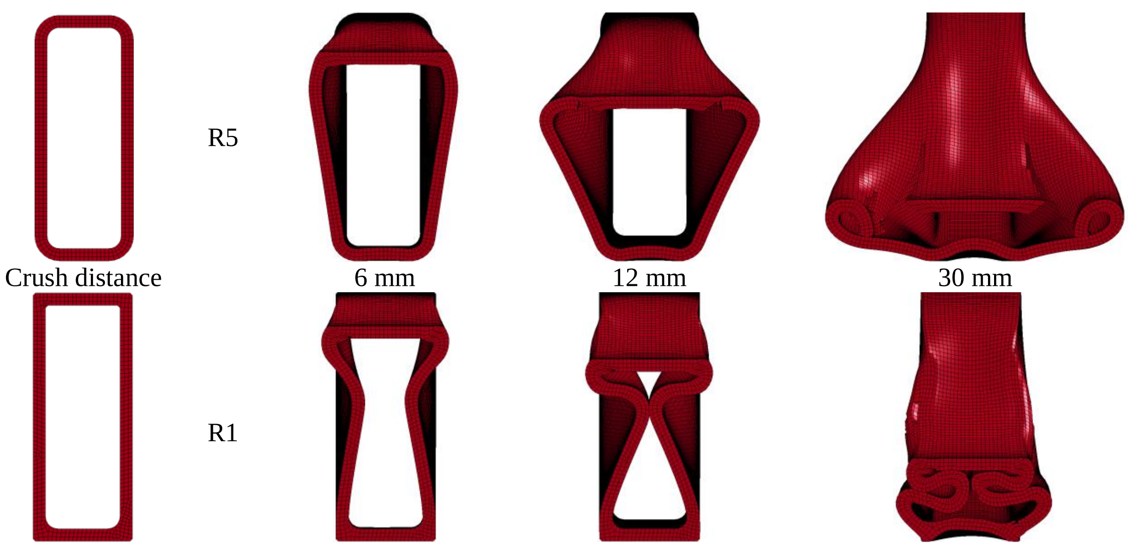

Figure 4. Lateral crush behavior for corner radius of 5 and 1 mm.

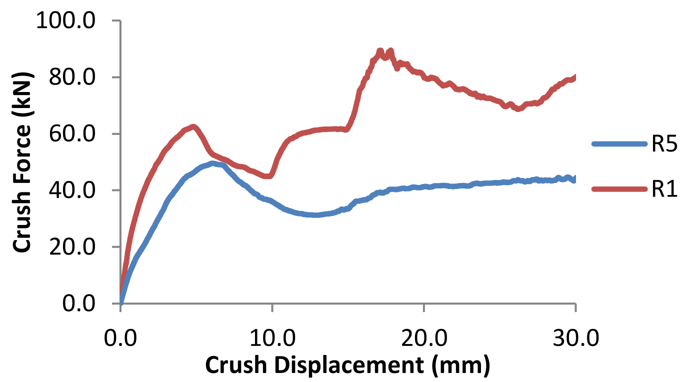

Figure 5. Crush force versus displacement for corner radius of 5 and 1 mm.

The final dimensions of the profile are shown in Figure 6. The die used to extrude the profile was a 2 port die with the extrusion welds deliberately located on the 20 mm faces where there is the lowest amount of deformation in the crush test. The die had an integral feeder ring to ensure good shearing and transverse weld quality. Standard industry scrap allowances were taken from the front and back of the extrusion. The lateral crush behavior of the extruded profile with the soft 6063GP alloy, compared to the simulation is shown in Figure 7.

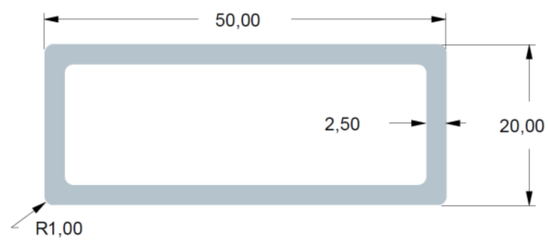

Figure 6. Dimensions of the profile [mm].

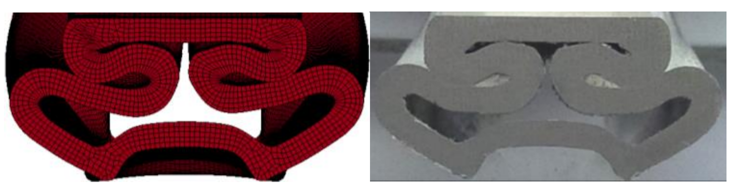

Figure 7. Lateral crush behavior of the extruded profile with 6063GP alloy, compared to the simulation.

In order to be able to rate the lateral crush behaviour of the alloys tested, it is necessary to look at the critical regions where material damage and fracture occur. Figure 8 shows the location of six critical (i.e. high strain) regions, while Figure 9 shows their plastic deformation as a function of crush distance and triaxiality. Triaxiality is a parameter used to define the stress state and can be described mathematically by the ratio of the hydrostatic component of the stress tensor to the equivalent stress. With this parameter, the type of deformation can be approximated (compression, shear, tensile, equi-biaxial) allowing evaluation of the fracture of a given material as a function of the stress state.

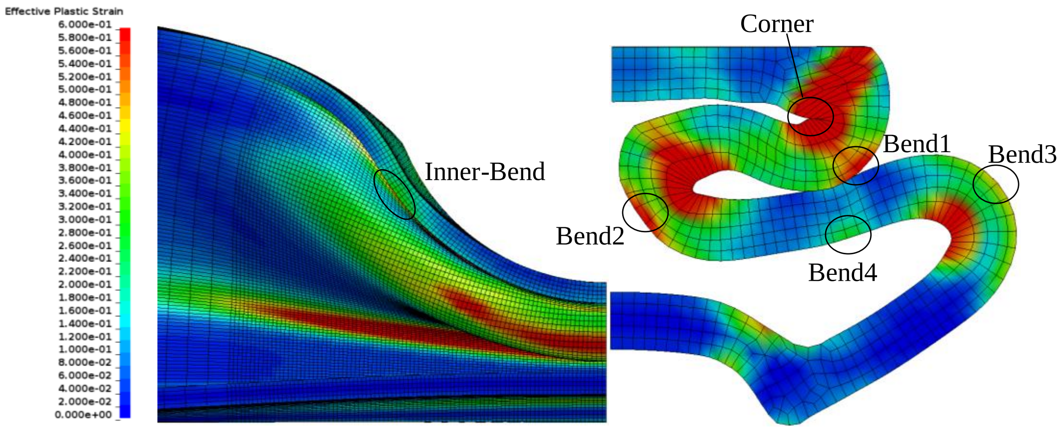

Figure 8. Six critical regions for failure in the crushed section.

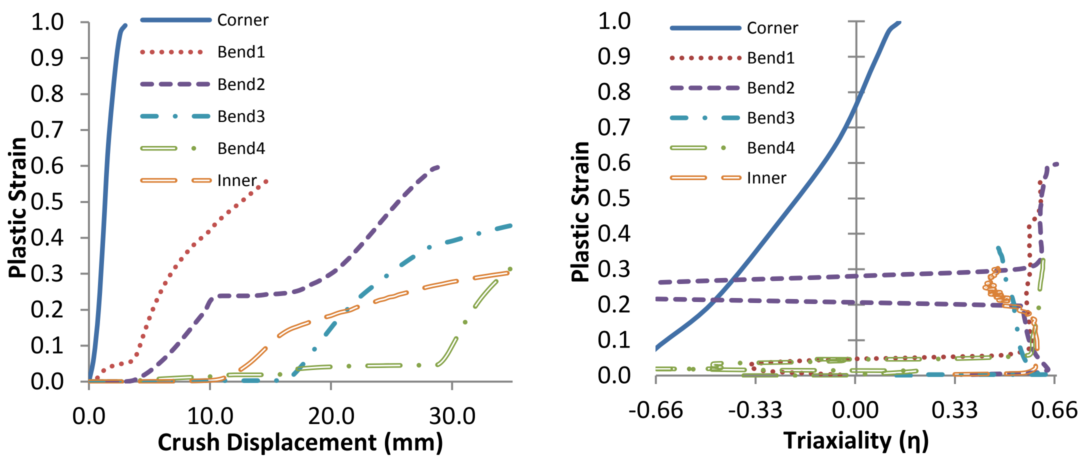

Figure 9. Fracture strains as a function of crush displacement and triaxiality for the critical regions.

Figure 10 shows a typical fracture strain ($\bar{\varepsilon}_f$) curve as a function of triaxiality (η), in this case, for plane stress conditions. The mechanical test type providing the corresponding stress state at each point is also illustrated. For the extruded profile used in this study, the highest strain in the crushed section is located at the top corner due to a high amount of both compression and shear deformation (low triaxiality). Depending on the amount of deformation in the shear mode, the corner region might not be as critical as, for example, the outer bends. For the outer bend regions, most of the stress state history is at a triaxiality value of ~0.6, which is expected for an outer surface of a bend with a plane stress and a plane strain state of deformation. Bends 1 and 2 undergo a small amount of compression during the crush. For Bend 1, this occurs at the beginning, before the vertical walls start to bend, while for Bend 2 it is when the walls meet each other at the center of the profile.

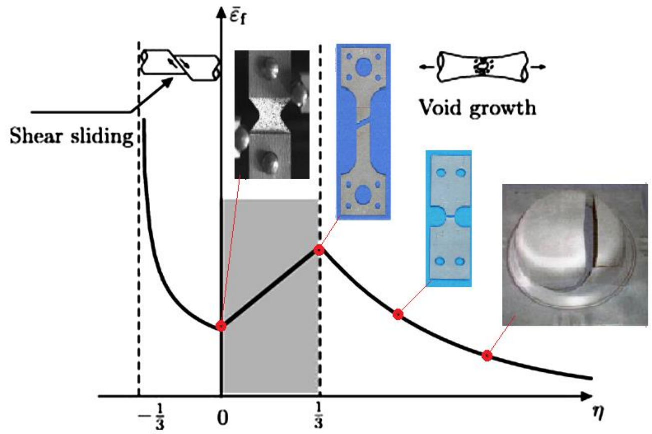

Figure 10. Typical failure curve for the plane stress condition and the equivalent mechanical tests.

Relevant Information Obtained from the Lateral Crush Test

In the lateral crush test, an important source of data is the force-displacement curve, where the main point of interest is the energy absorbed, as this is required to quantify a given material's crash performance. Figure 11a shows a typical crush force profile as a function of the crush distance for a material that exhibits no fracture. There is no repetitive crush behaviour, as in the case of an axial crush test where the folding of the profile gives a cyclical pattern in the load-displacement curve. Furthermore, unlike the axial crush test, the peak load is not at the beginning, but rather located around the mid-crush distance when the third bend (Bend 3) is created. In the lateral crush test, it is more appropriate to use the total absorbed energy as opposed to calculating a mean crush force as illustrated in Figure 11b.

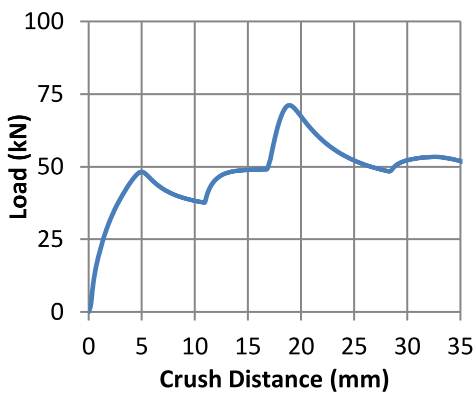

(a)

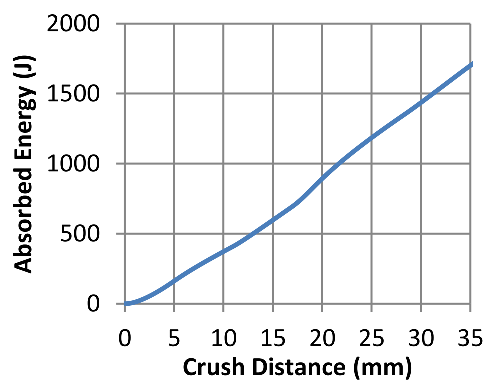

(b)

Figure 11. (a) Crush force as a function of crush distance; (b) Energy absorbed as a function of crush distance for 6063GP - peak aged

Another important piece of information that can be extracted from the lateral crush test is the degree of cracking exhibited by the material. This was assessed qualitatively by ranking the crushed tubes with a grade from 1 to 8, depending on the severity of the cracking, where a grade of 1 (i.e. no cracking) was deemed the best achievable. Table 2 presents examples of each of the eight grades.

Grade 2 represents a material that cracked only at Bend 4. If a crack at Bend 3 did not propagate during the crush test, then the top surface of the tube compressing down would have intiated a crack at the Bend 4 location. If, on the other hand, a Bend 3 crack had propagated during the crush, then the top tube surface would have simply pushed down on the inner fold ending in Bend 3 and no Bend 4 crack would have happened (this is shown in the sample of Grade 3). It is very likely that the localised deformation at Bend 4 was not acurately captured in the FE simulation due to the element size limitations on computation time. Smaller elements would have been necessary. Grades 3 to 8 represent an increase in cracking severity, with grade 8 translating to an entire fragmentation of the extruded profile.

Table 2. Lateral crush ratings; crush tube samples taken at central cross-section of deformed tube.

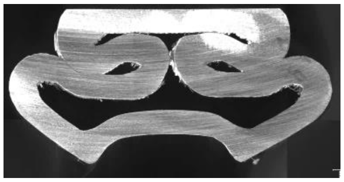		
Grade 1 No cracks	Grade 2 Small cracks – Bend 4	Grade 3 Small cracks – Bends 1 & 3
		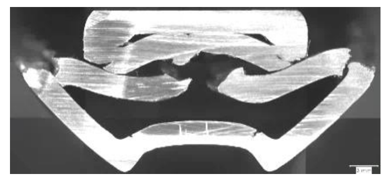
Grade 4 Deeper cracks – Bends 1 & 3	Grade 5 Deeper cracks – Bends 1 Small cracks – Bend 2 Complete failure – Bend 3	Grade 6 Deeper cracks – Bend 1 Complete failure – Bends 2 & 3
 	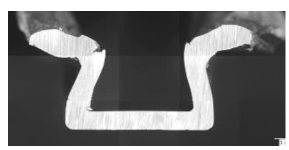 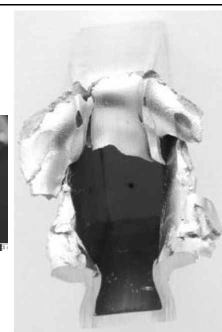	
Grade 7 Complete failure – Bends 1 to 3 and Inner-Bend	Grade 8 Entire profile fragmentation	

One can observe that in the crush ratings, fracture at Bend 3 occurs before fracture at Bend 2, even if the amount of strain computed by the FE model was less severe. This can be attributed to the different stress state histories for the two bends where Bend 2 was strained with compressive stresses for a certain amount of deformation (see triaxiality at Figure 9). As such, no fracture was observed at the corner due to the high level of deformation being mostly compressive.

Tensile Tests

Tensile testing was carried out on a 100-kN capacity MTS electromechanical test frame according to the ASTM E8 testing standard. Standard specimens (sheet-type) were machined from the 50 mm wide face of the profile in the extrusion direction. Two tensile tests were carried out for each conditions. A stereoscope with an image analysis routine was used to analyze grey tones and determine the final fracture area of each sample. The true fracture strain was measured using area reduction (i.e. the ratio of the fracture sample area to the initial cross-section), where the final sample area was measured on both sides of the fracture surface, and the average was taken as representative. The true fracture strain was calculated based on –ln(final area/initial cross-sectional area).

RESULTS

Microstructures

The extruded microstructures were typical of those encountered industrially for the same alloy types. Figure 12 presents the longitudinal grain structures for the four alloys. The more dilute alloys AA6063 and 6063HS, without significant additions of Mn or Cr, were fully recrystallized to a fine equiaxed grain size of ~150μ. The AA6061, containing a deliberate addition of Cr, was also fully recrystallised but in this case the final grain size was coarser (500 μ) and elongated in the extrusion direction. The AA6082 contained sufficient additions of Mn and Cr to promote an unrecrystallised grain structure with a thin recrystallised surface layer, which is a typical microstructure for commercially processed automotive grade AA6082. The differences in grain structure for the various alloys reflected the variations in Mn or Cr containing dispersoid particle distributions formed during billet homogenisation and the associated level of Zener pinning [1].

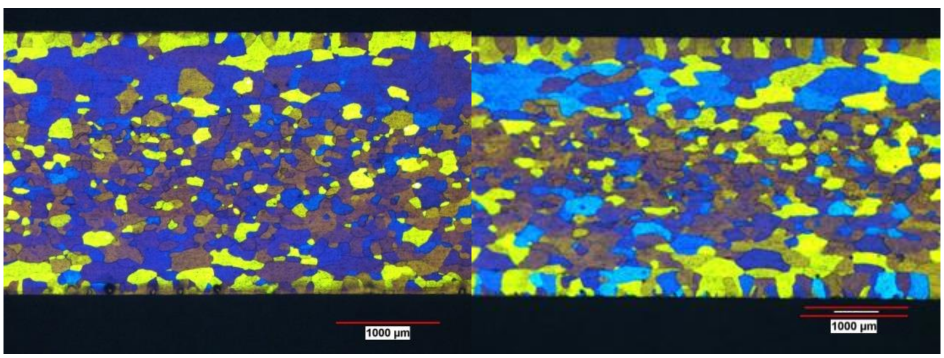

(a) 6063GP (b) 6063HS

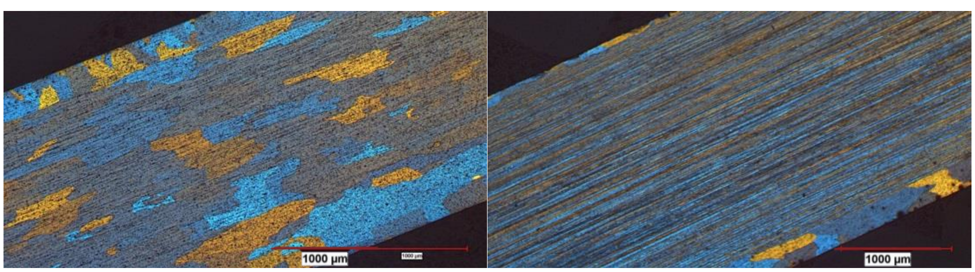

(c) AA6061 (d) AA6082

Figure 12. Extruded grain structures – Etched Barkers Reagent, longitudinal

Lateral Crush Testing

The appearance of the peak aged crushed samples for the four alloys and the corresponding load displacement curves are presented in Figure 13. The 6063GP was clearly the most ductile material and only exhibited small internal cracks (grade 2). The recrystallized 6063HS and AA6061with YS values of 257 and 280 MPa, respectively, both experienced severe fragmentation, whereas the stronger AA6082 with a fibrous grain structure was more ductile and only gave grade 6 cracking. The load displacement curves for the four alloys were similar in shape up to the peak load corresponding to bend 3, with the peak load increasing in line with the YS. However, the severe cracking that occurred beyond this point for the 6063HS and the AA6061 resulted in a decreasing crush load. In contrast the 6063GP and AA6082 both maintained a steady load after bend 3. Therefore in lateral crush, the strength and the extent of cracking both affect the total energy absorption

(a) 6063GP Grade 2 – 220 MPa YS

(b) 6063HS Grade8 – 257 MPa YS

© AA6061 Grade 8 – 280 MPa YS

(d) AA6082 Grade 6 – 301 MPa YS

Figure 13. Lateral crushed specimens in the peak-aged (175°C/8 hours) condition and the associated load versus crush displacement curve.

Figure 14(a) presents the qualitative crush grade ratings as a function of the true fracture strain for all alloy and temper variants. Clearly, as the fracture strain increased, the severity of cracking during crush decreased. It has already been established in the literature that ductility in bending can be evaluated with area reduction [10]; since lateral crush deformation is primarily in the bending mode, it is expected that the crush grade and ductility would display an inverse relationship. This also resembles the results obtained for axial crush experiments carried out by the current authors [1, 2, 3]. In general, for each alloy the overaged temper was the most ductile and tended to give a higher fracture strain and lower grading (less cracking) than the peak aged and underaged conditions. Comparing the different alloys, fracture strain and crush rating deteriorated with increasing alloy strength. The fibrous grained AA6082 was the exception to this trend, in line with the physical appearance of the crushed samples in Figure 13. Although it was the strongest alloy it exhibited superior ductility to the AA6061 and its data points were positioned in the middle of the grade-fracture strain distribution in Figure 14a.

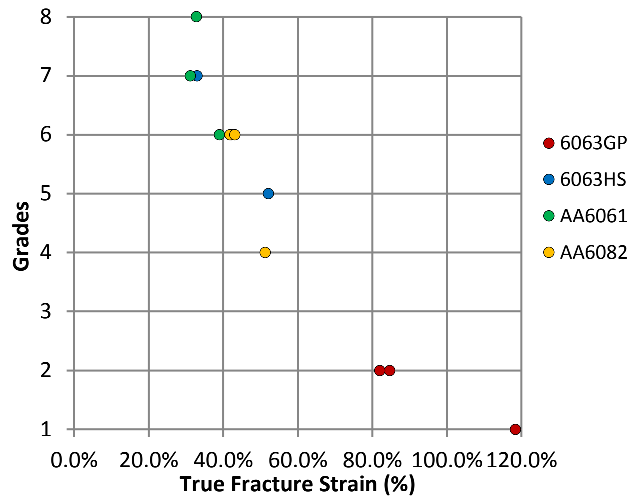

(a)

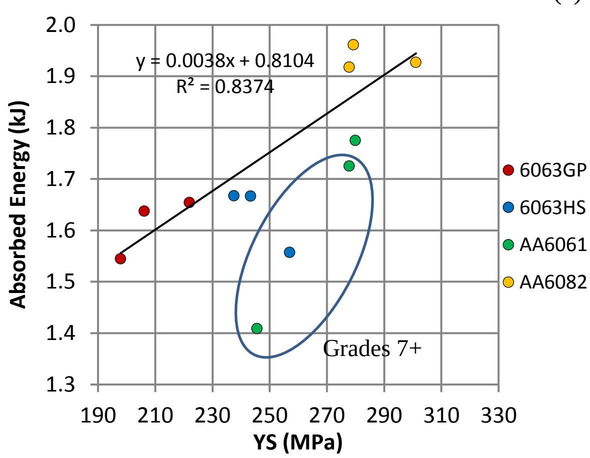

(b)

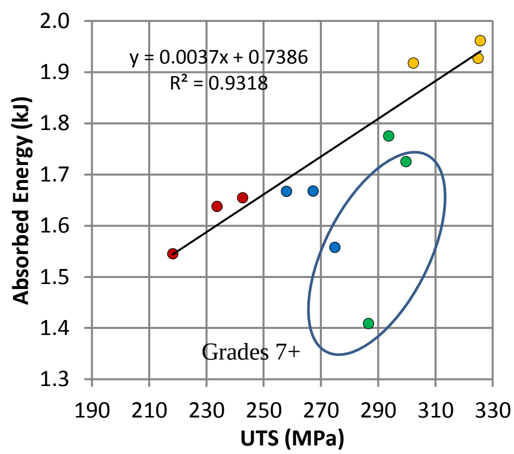

(c)

Figure 14. Crush rating as a function of the true fracture strain (a); energy absorbed as a function of the yield strength (b) and as a function of the ultimate tensile strength (c).

Figures 14(b) and 14(c) show the energy absorbed in the lateral crush test as a function of the yield strength (YS) and ultimate tensile strength (UTS). Both parameters can be used to predict the energy absorption potential when a limited amount of cracking occurs. A linear fit was applied to the data points corresponding to crush grades of 1-6 and the UTS resulted in a slightly better correlation as it allows for the effect work hardening occurring during deformation. This behaviour is somewhat different to previous findings for the case of axial crush where UTS was a much better predictor of energy absorbed[2]. The different behaviour probably reflects the overall higher strain levels encountered in axial crush. However, in the case of lateral crush, more severe cracking, reflected by inferior crush gradings (grade 7,8), significantly downgraded the energy absorption as shown by the circled points in Figures 14(b) and (c) for the peak-aged 6063HS and the underaged and peak aged AA6061. In fact for these grades, which corresponded to a fracture strain <35%, the rating was somewhat subjective as the onset of severe cracking modified the subsequent deformation behaviour until the end of the test. Therefore for this type of lateral crush test, the energy absorption is affected by the ductility of the material to a greater extent than in the case of an axial crush test [2], where the mean axial crush force was shown to demonstrate a linear relationship with the UTS even when severe cracking occurred during the test.

DISCUSSION

Given that there is a linear correlation between tensile strength and energy absorption, and that the fracture strain is a good indicator of crash ductility, then a plot of the fracture strain as a function of UTS should serve as a valuable tool for alloy/temper selection for lateral crash applications. Figure 15 presents such plots using UTS and YS. The individual points for each alloy are labelled to indicate the temper.

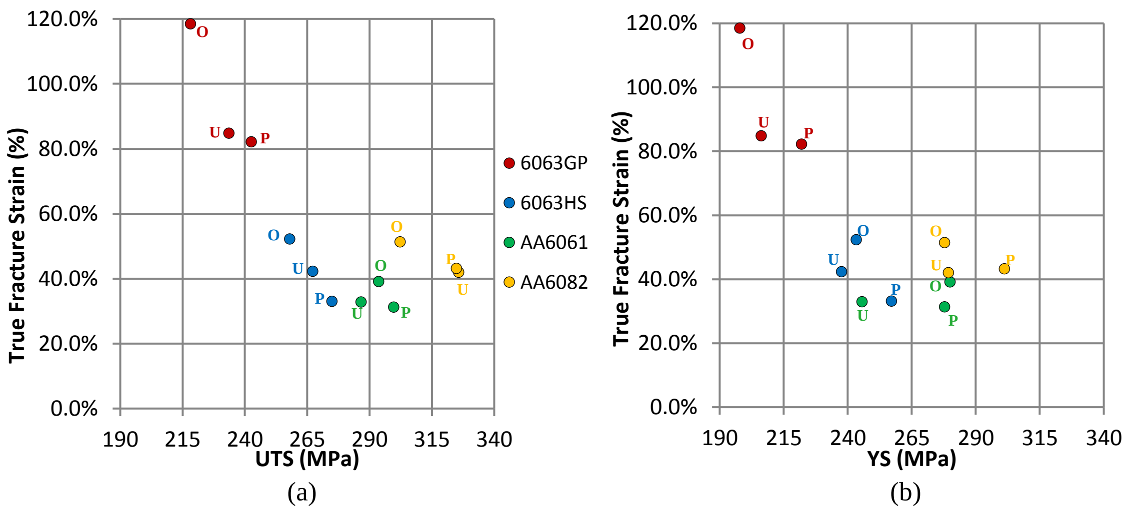

Figure 15. True fracture strain versus UTS (a) and YS(b) for all alloys considered in this work (U = underaged, P = peak-aged, O = overaged).

In general, for the fully recrystallised alloys, 6063GP, 6063HS and AA6061, the fracture strain decreased with increasing UTS with the data points distributed along the same curve. The application of an under or overaged temper reduced the strength and increased ductility somewhat but the points lay on the same general fracture strain – UTS curve offering no particular advantage to the overall crush behaviour. The non-recrystallized AA6082 gave a somewhat different behaviour and exhibited an increase in fracture strain compared to the recrystallized materials for a given strength level. Plotting the fracture strain values against yield strength, gave similar trends except that the effects of temper were more apparent. If strength below the peak aged condition is acceptable then for the same yield strength, over-aging tended to give superior ductility than under-aging.

For high levels of cracking, corresponding to fracture strain values <35% for the particular geometry used here, the trends in Figure 15 are somewhat idealised. As described above, at lower ductility levels the linear relationship between energy absorption and strength breaks down. Clearly such a condition should be avoided and to gain strength and avoid loss of ductility the use of a material such as AA6082 versus AA6061 appears advantageous. In this work the alloy change corresponded to a transition from recrystallized to fibrous grain structure caused by an increase in the dispersoid content of the alloy as described in earlier work[3]. Both factors could contribute to the increased ductility observed.

CONCLUSIONS

1. Using a combination of FE modelling and physical tests a lateral crush protocol was developed for a hollow extruded profile, capable of quantitative comparison of alloy and temper variants in terms of cracking sensitivity and energy absorption. Ductility critical deformation zones for lateral crush were identified which were used to quantify the cracking sensitivity.

2. Using a grading system established to quantify the extent of cracking during lateral crush, the extent of cracking was found to follow an inverse relationship with the true fracture strain

3. Energy absorption in lateral crush increases linearly with UTS, similar to axial crush. However, for severe levels of cracking (grade 7–8) this results in an overestimation due to disruption to the deformation mode which does not occur to the same extent in axial crush. In this study a minimum fracture strain value of 35% was required to avoid this condition.

4. With a press quench rate of 20°C/sec, the non-recrystallised AA6082 offered a step improvement in strength, ductility and lateral crush behaviour for a given strength level compared to a recrystallized AA6061 variant.

REFERENCES

[1] Parson, N. C., Beland J.F., Extrusions for Automotive Crash Applications, Proceedings of the Eleventh International Extrusion Technology Seminar, Chicago, 2016.

[2] Beland J-F., Parson N. C. Evaluation of the Axial Crush Performance of Al-Mg-Si Extrusions. Americas Conference on Aluminum Alloys, 2015, Toronto Canada, Paper 9121

[3] Parson, N. C., Fourmann, J., Beland, J-F., Aluminum Extrusions for Automotive Crash Applications. SAE International 2017 Detroit, paper 2017-01-1272.

[4] Rebuffet O., Morère B., Magni B. and Bompard S., Aluminium Extrusion Alloy Selection for Crashworthiness Energy Absorption and Failure, Society of Automotive Engineers, 2002.

[5] Royset J., Tundal U., Reiso O. and Furu T., Al-Mg-Si Alloys with Improved Crush Properties, Proceedings of the Nine International Aluminum Extrusion Technology Seminar, 2008.

[6] Strano M., Villa A., Mussi V., Design and manufacturing of anti-intrusion bars made of aluminium foam filled tubes, International Journal of Material Forming, 2013, 6(1), p. 153.

[7] Robert Long C., Analysis of a Car Door Subjected to Side Impact, Thesis, University of Cape Town, Blast Impact and Survivability Research Unit Department, 2016.

[8] Ho Yoon T, Kim H., Heo C., An experiment and FE simulation for the development of a SPFC1180 AHSS one-body door impact beam about a car side collision, International Journal of Precision Engineering and Manufacturing, 2016, 17(1), p. 81.

[9] Gomes Mota Rebelo P., Design Study of a Side Intrusion Beam for Automotive Safety, Thesis, University of Lisbon, November 2016.

[10] Datsko J., Yang C., Correlation of Bendability of Materials with their Tensile Properties, The University of Michigan, Industry Program of the College Engineering, IP-401, 1959

[11] IIHS Side Impact Crashworthiness Evaluation – Crash Test Protocol, Insurance Institute for Highway Safety, July 2017.